Influence of Side Chain Hydrolysis on the Evolution of Nanoscale Roughness and Porosity in Amine-Reactive Polymer Multilayers

Matthew C. D. Carter,^{1,†} Matthew S. Wong,¹ Fengrui Wang,¹ and David M. Lynn^{1,2,*}

¹Department of Chemistry, 1101 University Avenue, University of Wisconsin—Madison, Madison, Wisconsin 53706 and ²Department of Chemical and Biological Engineering, 1415 Engineering Drive, University of Wisconsin—Madison, Madison, Wisconsin 53706; [†]Current address: The Dow Chemical Company, Core Research & Development, 400 Arcola Rd, Collegeville, Pennsylvania 19426; *E-mail: dlynn@engr.wisc.edu

ABSTRACT: We report the influence of side chain hydrolysis on the evolution of nanoscale structure in thin films fabricated by the reactive layer-by-layer (LbL) assembly of branched poly(ethylenimine) (PEI) and poly(2-vinyl-4,4-dimethylazlactone) (PVDMA). LbL assembly of PEI and PVDMA generally leads to the linear growth of thin, smooth films. However, assembly using PVDMA containing controlled degrees of side chain hydrolysis leads to the growth of thicker films that exhibit substantial nanoscale roughness, porosity, and have resulting physicochemical behaviors (e.g., superhydrophobicity) that are similar to those of some thicker PEI/PVDMA coatings reported in past studies. Our results reveal that the degree of PVDMA partial hydrolysis (or carboxylic acid group content) influences the extent to which complex film features develop, suggesting that ion-pairing interactions between hydrolyzed side chains and amines in PEI promote the evolution of bulk and surface morphology. Additional experiments demonstrate that these features likely arise from polymer/polymer interactions at the surfaces of the films during assembly, and not from the formation and deposition of solution-phase polymer aggregates. When combined, our results suggest that nanoporous structures and rough features observed in past studies likely arise, at least in part, from some degree of adventitious side chain hydrolysis in the PVDMA used for film fabrication. Our results provide useful insight into molecular-level features that govern the growth and structures of these reactive materials, and provide a framework to promote nanoscale morphology reliably and reproducibly. The principles and tools reported here should prove useful for further tuning the porosities and tailoring the physicochemical behaviors of these reactive coatings in ways that are important in applied contexts.

Introduction

Porous polymer-based coatings are useful in a range of advanced applications, including separation and filtration, drug delivery, and as solid-phase heterogeneous catalyst supports. ¹⁻⁸ The versatility of this class of materials results, at least in part, from the ability to tune pore size, shape, and functionality by manipulating the chemical structures and physical properties of the constituent polymers. Porous polymer coatings can be fabricated using a range of approaches, including phase separation, imprinting, or templating techniques, among others. ^{4,6-8} Layer-by-layer (LbL) assembly has also recently emerged as a useful approach for the design of porous polymer films, and can yield composite polymer-based materials that exhibit a broad range of pore types, sizes, and morphologies. ⁹⁻²⁵ LbL assembly also offers the potential to tune film features in new ways, because the compositions, thicknesses, and architectures of these materials can be influenced by myriad process parameters, including the structures and properties of the constituent polymers and the number of assembly cycles. ²⁶⁻³¹

Although a general understanding of the physicochemical behaviors of LbL polymer coatings has been established, a number of complex factors—including the intermixing or interdiffusion of polymer layers³²⁻³⁴ and other structural reorganizations that can occur during^{21,23,25} or after^{9-18,20,22,35,36} film fabrication—can influence morphology, surface roughness, and ultimately lead to the generation of interconnected pores on micro- and nanometer scales.³⁷⁻⁴⁰ These inherent complexities are less well-understood, but they often result in the unexpected discovery of new classes of coatings and interfaces with features or new behaviors that are of interest in many fundamental and applied contexts. The work reported here was motivated by understanding factors that influence the formation of nanoscale roughness and porosity that develop in thin films fabricated using 'reactive' or 'covalent' LbL assembly.^{37,40}

Past studies from our group have demonstrated that interfacial reactions between aminereactive poly(2-vinyl-4,4-dimethylazlactone) (PVDMA) and the amine-containing polymer poly(ethylenimine) (PEI) can drive LbL assembly into films that are either thin, smooth, and relatively featureless at the nanometer scale, 41-43 or thicker (micrometer-scale) with significant nano- and microscale surface features and substantial nanoscale porosity. 44-47 These PEI/PVDMA multilayers are potentially useful in at least three ways: (i) similar to other LbL processes, these materials can be fabricated on a broad range of topologically complex substrates, 42 (ii) the assemblies that result exhibit superior stabilities in complex chemical environments owing to the presence of hydrolytically stable amide-based cross-links, 45 and (iii) the resulting films contain residual azlactone groups that can be used to further functionalize and tailor bulk and surface properties by reactions with a range of nucleophiles.⁴⁷ These useful properties make PEI/PVDMA multilayers a versatile platform for the elaboration of a broad range of new functional materials, including tailored biointerfaces, 42,43 reactive polymer-based capsules, 48 and new types of chemical and biomolecular sensors. 48 More recently, chemically reactive PEI/PVDMA films with substantial degrees of nanoscale roughness and porosity have made possible the design of surface coatings with extreme wetting behaviors (e.g., superhydrophobicity, underwater superoleophobicity, etc.), 44,45,47 including new types of 'bulk' superhydrophobic coatings that can protect and sustain the long-term release of water-sensitive molecules. 49 In addition, appropriately functionalized porous PEI/PVDMA multilayers have been used as matrices for the design of anti-fouling, 'slippery' liquid-infused porous surfaces (SLIPS) that can prevent surface fouling by fungi and bacteria.⁴⁶

While the physiochemical properties of porous PVDMA/PEI materials have been exploited in the context of several potential applications, the processes that lead to porosity

during LbL assembly—or that can be used to control the extents or the scales on which they occur—remain poorly understood. Although past studies have reported multilayer assembly procedures that can be used to promote the evolution of roughness and porosity, ^{44,49,50} the molecular-level interactions or other physical parameters that influence structure formation are unknown. Here, we report physicochemical investigations into interactions and processes that lead to the development of micro- and nanoscale structure and porosity in PEI/PVDMA-based multilayers and elucidate molecular design principles that can be used to control, influence, or tune the porous nature of the material morphology.

We demonstrate that the presence of hydrolyzed azlactone groups in PVDMA plays an important role in promoting the generation of porosity and roughness: while the assembly of PVDMA and PEI leads to the linear growth of thin, smooth films that are devoid of nanoscale features, assembly using PVDMA synthesized to contain controlled degrees of side chain hydrolysis leads to the growth of thicker films that exhibit substantial nanoscale roughness, porosity, and resulting physicochemical behaviors are similar to those reported in past studies. When combined, our results suggest that porous structures and rough features observed in past studies likely arose, at least in part, from some degree of adventitious side chain hydrolysis in the materials used for film fabrication. Because the hydrolysis of azlactone groups yields carboxylic acid-containing side chains, our observations lead to a proposed physical picture of nanostructure formation and the evolution of rough/porous morphologies that includes molecular-level interactions influenced or driven by acid/base ion-pairing interactions with PEI during LbL assembly. These observations and the results of other related experiments reported here are consistent with this view, and provide a framework for understanding, tuning, and exploiting the range of competing interactions that control film growth and lead to changes in film morphology.

Our results provide insights, guiding principles, and new experimental tools that may prove useful in further tuning and tailoring the properties and behaviors of these reactive coatings.

Materials and Methods

Materials. Branched poly(ethyleneimine) (PEI; MW ~25,000), azobisisobutyronitrile (AIBN, recrystallized once from methanol), decylamine (95%+), concentrated hydrochloric acid (HCI, 37%, ACS reagent), tetrahydrofuran (THF, HPLC grade, >99.9%), dichloromethane (DCM, ACS grade), and hexanes (technical grade), were purchased from Sigma-Aldrich (Milwaukee, WI). Inhibitor Removal Resin was purchased from Alfa Aesar (Radnor, PA). 2-Vinyl-4,4-dimethylazlactone (VDMA) was a kind gift from Dr. Steven M. Heilmann (3M Corp., Minneapolis, MN) and was fractionally distilled under reduced pressure (B.P. ~22 °C at ~500 mTorr; clear mobile liquid at room temperature). The middle distillation fraction was collected as a clear, non-viscous, colorless oil. Butylated hydroxytoluene (BHT, 500 ppm) and triethylamine (NEt₃, 1000 ppm) were added, and the monomer was stored at -18 °C in the dark prior to use. Water with a resistivity of 18.2 MΩ•cm was obtained from a Millipore filtration system. Unless otherwise noted, materials were used as received.

General Considerations. 1 H NMR spectroscopy for VDMA, P1, and P1_x derivatives was performed in CDCl₃ using a Bruker Avance-500 spectrometer. A relaxation delay of 10 s was used for all polymers and all spectra were referenced relative to the residual proton peak of CHCl₃ (δ 7.26 ppm). Gel permeation chromatography was performed using a Viscotek GPC Max VE2001 equipped with two Polymer Laboratories PolyPore columns (250 mm × 4.6 mm), a TDA-302 detector array, and THF as the eluent at a flow rate of 1 mL/min at 40 °C. The

instrument was calibrated using 10 narrow dispersity polystyrene standards with M_n = 0.580-377.4 kg/mol (Agilent Technologies, Santa Clara, CA). Attenuated total reflectance (ATR) IR measurements were obtained using a Bruker Tensor 27 FTIR spectrometer outfitted with a Pike Technologies Diamond ATR stage (Madison, WI). Data were analyzed using Opus Software version 6.5 (Bruker Optik GmbH). Spectra were collected at a resolution of 2 cm⁻¹ and are presented as an average of 16 scans. Data were smoothed by applying a nine-point average and baseline-corrected using a concave rubberband correction (10 iterations, 64 points). Optical thicknesses of films deposited on silicon substrates were determined using a Gaertner LSE ellipsometer (632.8 nm, incident angle = 70°) and data were processed using the Gaertner ellipsometer measurement software. Thicknesses were calculated assuming a refractive index of 1.577, and were determined in at least five different locations for three replicate films. All films were dried under a stream of filtered compressed air prior to thickness measurements. Contact angle measurements were made using a Dataphysics OCA 15 Plus contact angle goniometer at ambient temperature with 4 μL of 18.2 MΩ Millipore water in at least 3 different locations on each film. Scanning electron micrographs were acquired using a LEO-1550 VP field-emission SEM operating with an accelerating voltage of 1 kV. Film samples were coated with a thin layer of gold prior to imaging; polymer and rinse solutions on silicon chips were imaged without gold coating. Digital pictures were acquired using a Canon PowerShot SX130 IS digital camera. Compressed air used to dry samples was filtered through a 0.2 µm membrane syringe filter

Synthesis of Poly(2-Vinyl-4,4-Dimethylazlactone) (PVDMA) [Polymer P1]. The following general procedure yields unhydrolyzed PVDMA when freshly distilled monomer is used. VDMA was first passed through two Pasteur pipet columns of Inhibitor Removal Resin (~3.5 cm height)

followed by a Pasteur pipet column of silica gel (\sim 2 cm height) to remove BHT and NEt₃, respectively. VDMA (2.05 g, 14.8 mmol), AIBN (24.4 mg, 0.148 mmol), and ethyl acetate (6.0 mL, dried over MgSO₄ and filtered through a 0.2 μ m PTFE syringe filter) were added to an oven-dried 25 mL round-bottomed flask, sealed, and sparged with nitrogen for 15 minutes before being placed into an oil bath at 60 °C. After 24 hours, the flask was cooled to room temperature, the mixture was diluted with \sim 4 mL of DCM and precipitated into \sim 300 mL of hexanes at room temperature. The resulting white solid was collected by vacuum filtration and then dried under high vacuum to constant weight to give **P1**. ¹H NMR (400.180 MHz, CDCl₃, δ ppm): 2.71 (s, 1H), 2.16-1.79 (m, 2H), 1.37 (s, 6H). ATR IR (cm⁻¹): 1818 (C=O azlactone), 1671 (C=N azlactone), 1203 C-O-C (azlactone). A representative ¹H NMR spectrum is shown in Figure S1 of the Supporting Information.

Partial Hydrolysis of PVDMA [Polymer P1_x]. Polymer P1 was partially hydrolyzed to different degrees to yield P1_x, where x indicates the final degree of partial hydrolysis, using the following general procedure. A sample of P1 (~35 mg) was weighed into a 6 mL glass vial with a stir bar and dissolved in 0.75 mL THF to give a clear solution. A 0.1 M HCl solution in THF/H₂O was freshly prepared by adding 82.1 μ L of concentrated HCl to 9.918 mL of THF using a volumetric pipet (in this solution, [H₂O] = 0.455 mol/L). A pre-determined volume of this solution targeting a specific degree of azlactone hydrolysis was added, with stirring, to the vial containing the P1 solution, and the vial was sealed. The mixture turned bright yellow immediately after addition of the acid solution, and the vial was left to stir overnight at room temperature. The yellow color generally dissipated after several hours, but often persisted for samples with high degrees of hydrolysis (e.g., ~20% or greater). The polymer was precipitated

into \sim 15 mL of hexanes and collected by centrifugation. The resulting $P1_X$ derivatives were dried under high vacuum overnight to yield white solids. A representative 1H NMR spectrum of partially hydrolyzed PVDMA is included in Figure S1. THF solvent (HPLC grade) was used for this procedure and was not necessarily anhydrous; the actual degree of hydrolysis was therefore often higher than targeted. The final degrees of hydrolysis for $P1_X$ derivatives were determined using quantitative ^{13}C NMR spectroscopy as described in the next section.

Characterization of Degrees of Hydrolysis of PVDMA by Quantitative ¹³C NMR Spectroscopy. Quantitative ¹³C NMR spectroscopy was performed using a Bruker Avance 3 spectrometer equipped with a liquid He-cooled DCH cryoprobe. Samples were dissolved at ~2 wt% in acetone- d_6 and all spectra were referenced relative to the residual carbonyl carbon in acetone- d_6 ($\delta = 206.26$ ppm). Acquisition parameters were adapted from the literature⁵¹ and data were acquired using a relaxation delay of 10 s and an average of 1024 scans. The degree of hydrolysis was calculated using the integration of the peaks corresponding to the quaternary carbons in the ring-closed and ring-opened form of the azlactone ring, and by the equation Percent Hydrolysis = $[I_{ring-opened} / (I_{ring-opened} + I_{ring-closed})]$. For example, for P1_B, Percent Hydrolysis = [0.20 / (0.20 + 1.00)] = 0.167 or 16.7%. The associated error in degree of hydrolysis was obtained by assuming an error of $\pm 5\%$ in the value of each integral, and by propagating through the percent hydrolysis calculation. Representative ¹³C NMR spectra used to determine the degree of hydrolysis of polymers used in this study are included in Figure S2.

Layer-by-Layer Assembly of PEI/P1 and PEI/P1_x Coatings. Multilayers of PEI/P1 or PEI/P1_x were fabricated on glass or silicon substrates (\sim 1 x 4 cm, five total substrates for each

condition; pre-cleaned with methanol and acetone) using the following general procedure reported in past studies for the fabrication of nanoporous PEI/PVDMA films: 44,50 (i) substrates were submerged in a solution of PEI (\sim 0.87 mg/mL; 20 mM in acetone with respect to the polymer repeat unit) for 20 s; (ii) substrates were removed and immersed in an initial acetone bath for 20 s, followed by a second acetone bath for 20 s; (iii) substrates were submerged in a solution of P1 or P1_X (\sim 2.8 mg/mL; 20 mM in acetone with respect to the polymer repeat unit for P1, \sim 3.1 mg/mL for P1_X) for 20 s; and (iv) substrates were removed and rinsed again using the procedure outlined under step (ii). This cycle was repeated 35 times, without changing the rinse solutions to yield films 35 bilayers thick. After fabrication, films were washed copiously with acetone from a spray bottle and then dried under a stream of compressed air. Films were stored in a vacuum desiccator prior to use. To functionalize residual azlactone groups with decylamine, films were incubated overnight in solutions of decylamine (20 mg/mL) in THF at room temperature. After incubation, films were rinsed with THF and then dried under a stream of compressed air.

Characterization of Polymer Aggregates Formed During Film Fabrication. In experiments designed to characterize the presence of polymer aggregates in the polymer dipping solutions and the rinse solutions used for film fabrication, multilayer films were assembled using the above procedure and a model $P1_X$ polymer containing $22.5 \pm 1.4\%$ hydrolyzed side chain groups. After film fabrication, two drops of solution from each polymer solution vial (PEI and $P1_X$) were cast onto silicon substrates, the acetone was allowed to evaporate off at room temperature, and the remaining material was imaged by SEM. In separate experiments designed to investigate the effect of polymer solution 'carry-over' and subsequent co-mixing and

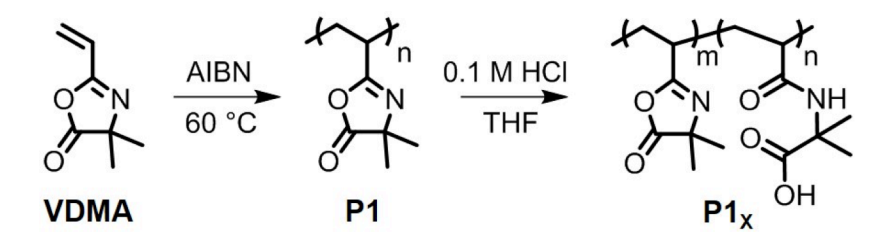
aggregation of PEI and $P1_X$ polymers in vials during fabrication, the dipping procedure described above was followed, with the exception that the rinse solutions were replaced with fresh acetone after every rinse step. After film fabrication, a drop of solution from each polymer solution vial was cast onto a silicon substrate for SEM imaging, as described above.

Results and Discussion

The presence of hydrolyzed azlactone groups impacts film growth

Past work has demonstrated that PEI/PVDMA multilayers can be fabricated in ways that lead to either (i) thin and smooth films that are optically transparent, 41-43 or (ii) thicker films that are optically opaque and exhibit micro- and nanoscale roughness and substantial internal porosity. 44-46,49,50 The approaches used to fabricate these materials all have, in common, protocols that involve the iterative and alternating immersion of substrates into solutions of PEI and PVDMA in acetone, with intervening exposure to acetone rinse solutions. As described above, past studies reported procedures and process parameters that could be used to bias film growth toward the evolution of substantial nanoscale roughness and porosity. For example, the use of (i) PVDMA synthesized in the presence of cyclic oligomers of VDMA^{44,52} and (ii) protocols that do not involve the regular replacement of polymer and rinse solutions during fabrication, 45,46,49,50 have both been used to fabricate nanoporous and topographically complex coatings that exhibit superhydrophobicity, superhydrophilicity, or underwater superoleophilicity when functionalized with appropriate amine-based nucleophiles (e.g., hydrophobic or hydrophilic amines, as discussed below). 44,45,49,50

During the course of our current studies, however, we occasionally encountered samples of PVDMA, synthesized using previously reported protocols, that either did not lead to films



Scheme 1. General scheme showing the polymerization of VDMA to P1, and subsequent partial-hydrolysis using aqueous HCl in THF at room temperature to yield $P1_X$ derivatives.

with substantial roughness or porosity, or lead to films that were porous and rough, but that did not exhibit some anticipated functional properties (e.g., extreme wetting behaviors) after postfabrication functionalization. Those results prompted additional spectroscopic characterization and comparisons of samples of PVDMA used in those experiments that revealed evidence of variable levels of side chain azlactone hydrolysis in polymers synthesized under otherwise similar conditions (these results are discussed in greater detail below). The ring-opening hydrolysis of the azlactone groups in PVDMA yields carboxylic acid functionality, as shown in Scheme 1. For the purpose of clarity in the discussion below, we refer from here on to PVDMA as 'polymer P1' and denote PVDMA containing specific mole fractions of hydrolyzed side groups, as depicted in Scheme 1, as 'polymers $P1_X$ ', where 'x' denotes a specific mole fraction of hydrolyzed repeat units. Our initial observations from those characterization studies described above suggested that the presence and variability in the number of hydrolyzed azlactone groups in these polymers could play a role in the evolution of rough and nanoporous morphologies observed in PEI/PVDMA multilayers and, thus, motivated the additional series of synthetic and physicochemical characterization studies described below.

In a first series of experiments, we sought to synthesize samples of P1 and provide insight into factors that could lead to side chain hydrolysis. To initiate these studies, we prepared

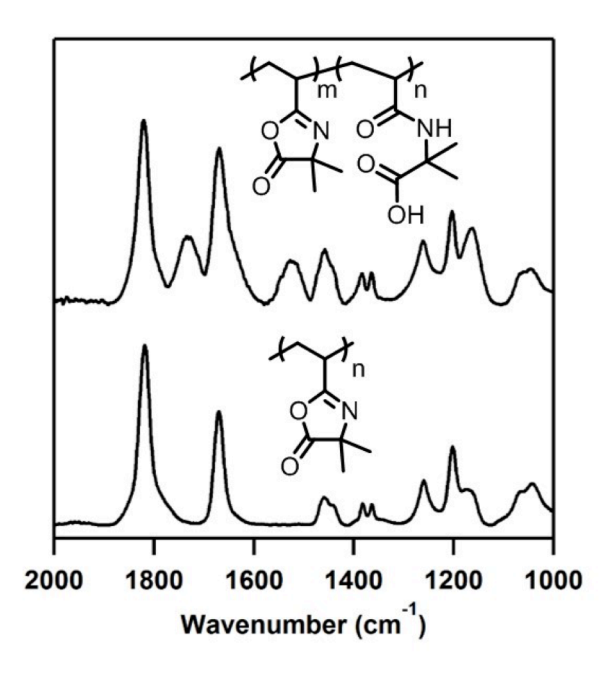


Figure 1. ATR IR spectra for **P1** (bottom) and partially hydrolyzed **P1**_X (top). The peaks corresponding to the azlactone carbonyl (C=O, 1818 cm⁻¹) and azlactone imine (C=N, 1671 cm⁻¹) stretches are observed in the spectra of both **P1** and **P1**_X. Carboxylic acid carbonyl stretching (C=O, 1734 cm⁻¹) and amide bending (N-H, 1528 cm⁻¹) peaks associated with hydrolyzed azlactone rings are present in the spectrum of **P1**_X only.

samples of **P1** using VDMA monomer that was freshly distilled (Scheme 1; see Materials and Methods for additional details). The use of freshly distilled monomer reproducibly yielded **P1** that did not contain hydrolyzed side chain groups,⁵³ whereas samples of **P1** synthesized using monomer that was not freshly distilled often lead to polymers with varying degrees of side chain hydrolysis (i.e., **P1**_X, Scheme 1), as determined by characterization using FTIR. Figure 1 shows the IR spectra of **P1** and a representative sample of **P1**_X polymerized using monomer that was not freshly distilled, similar to that used in past studies to fabricate nanoporous PEI/PVDMA films. The diagnostic azlactone carbonyl (C=O, 1821 cm⁻¹) and azlactone imine (C=N, 1672 cm⁻¹) stretches are present in both spectra.⁵⁴ However, the spectrum of **P1**_X also reveals a carboxylic acid carbonyl (C=O, 1734 cm⁻¹) stretch and an amide bending mode (N-H, 1528 cm⁻¹)

characteristic of hydrolyzed side chain groups. Evidence of a ring-opened amide carbonyl peak can be observed as a shoulder on the C=N peak in the $P1_X$ spectrum (C=O, ~1650 cm⁻¹).⁵⁴ We did not observe the presence of hydrolyzed VDMA monomer in samples that were not freshly distilled by NMR (data not shown), nor did we detect substantial differences in the water content of freshly distilled VDMA (735 ± 97 ppm) and samples that were not freshly distilled (645 ± 76 ppm) by Karl-Fisher titration.

When combined, the results above suggest that the hydrolyzed units in samples of P1_x do not arise from the incorporation of hydrolyzed monomer or the presence of water (that could lead to hydrolysis) during polymerization. We speculate that the partial hydrolysis observed in these samples and others used in past studies may be promoted by the presence of other, currently unidentified acidic impurities that may exist as a by-product of monomer synthesis⁵⁴ or that can form upon the standing and storage of VDMA, or by impurities introduced by the addition of cyclic oligomers of VDMA⁵² used to prepare PVDMA in some past studies.⁴⁴ We note that it is also possible for side chain hydrolysis to occur after polymerization and upon storage by exposure to water, heat, or other acidic and basic species (i.e., in wet or dry samples of P1). The further identification of specific impurities that could lead to hydrolysis was not a primary aim of this study.

We performed a series of initial experiments using the P1 and $P1_X$ polymers characterized above to fabricate PEI/PVDMA multilayers following a protocol used in past studies to fabricate rough and nanoporous coatings. ^{44-46,49,50} In brief, this protocol involved the iterative immersion of substrates into a solution of PEI, two subsequent rinse solutions, then a solution of $P1_X$, and finally two additional rinse solutions to fabricate what we refer to as one PEI/PVDMA 'bilayer' (see Figure 2A; this basic cycle was repeated multiple times, as desired,

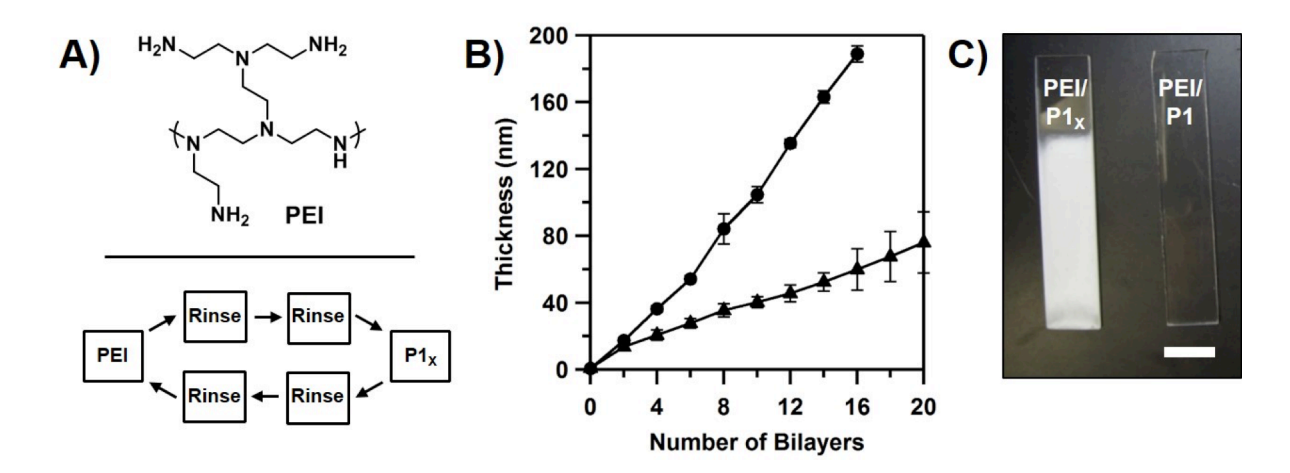


Figure 2. (A) Chemical structure of branched poly(ethylenimine) (PEI, top) and schematic showing the process flow of the LbL approach used to fabricate the films investigated in these studies (bottom). (B) Film growth profiles for PEI/P1 (filled triangles) and PEI/P1_X (filled circles) films fabricated on planar silicon substrates, as characterized by ellipsometry. Error bars represent the standard deviation of at least five measurements on five separate films. (C) Photos showing the physical appearance of 35 bilayer thick PEI/P1_X and PEI/P1 films assembled on glass substrates. Scale bar = 1 cm.

to promote LbL growth. All solutions were prepared using acetone; see Materials and Methods for full details). Figure 2B shows the increase in optical thickness, as determined by ellipsometry, for PEI/P1 and PEI/P1_X films fabricated on reflective silicon substrates as a function of the number of bilayers deposited. These results reveal PEI/P1 films (filled triangles) to grow relatively slowly and with a linear deposition profile up to 20 bilayers, to an average thickness of ~75 nm. This film growth profile is similar to those reported in several past studies on the LbL assembly of PEI/PVDMA films.⁴¹ In contrast, PEI/P1_X films (filled circles) increased in thickness much more rapidly, with a profile that was also roughly linear but with a greater slope, for up to 16 bilayers and to an average thickness of ~190 nm under otherwise identical conditions (these films became optically opaque after 16 bilayers were deposited, preventing further analysis of film growth using ellipsometry).

Figure 2C shows digital photographs of PEI/P1 and PEI/P1_X films 35 bilayers thick fabricated on glass substrates under otherwise identical conditions. PEI/P1 films fabricated under these conditions (right) were smooth and optically uniform and transparent; PEI/P1_X films (left) were optically opaque and exhibited surface roughness that was apparent to the naked eye, similar to rough and nanoporous coatings reported in other past studies. 44-46,49,50 When combined, these results suggested that the presence of hydrolyzed azlactone functionality in PVDMA could contribute to the evolution of micro- and nanostructures during LbL assembly. Additional characterization of P1 and P1_X by gel permeation chromatography revealed similar molecular weights and dispersities (see Figure S3), suggesting that the differences shown in Figure 2 do not arise from large differences in these macromolecular parameters.

In all further studies described below, we performed experiments using samples of $P1_X$ synthesized by the intentional and controlled hydrolysis of P1 to investigate the influence of hydrolysis and differences in carboxylic acid group content on film growth and morphology.

Influence of the degree of side chain hydrolysis on film growth, morphology, and properties

Scheme 1 above shows our approach to the synthesis of P1_X derivatives having different degrees of partial side chain hydrolysis. Treatment of solutions of P1 in THF with a known amount of water and in the presence of an acid catalyst yielded polymers P1_A, P1_B, P1_C, and P1_D, as shown in Table 1. (We note here that the addition of water alone to solutions of P1 in THF, followed by overnight incubation, did not induce any azlactone hydrolysis, as monitored by IR spectroscopy). We determined the percent hydrolysis generated under these conditions using

Table 1. Percentage of Side-chain Hydrolysis (Hydrolysis, %) and Azlactone: Acid IR Peak Height Ratio for P1_x Copolymers Synthesized in this Study.

Name	Hydrolysis, % a	Azlactone:Acid ^b
P1	0	n/a
P1 _A	13.8 ± 0.9	7.37
P1 _B	16.7 ± 1.1	4.54
P1 _C	25.9 ± 1.6	3.57
P1 _D	35.5 ± 2.1	3.05

^aPercentage of side-chain hydrolysis, as determined by quantitative ¹³C NMR spectroscopy; ^b[Azlactone]:[Acid] ratio as determined by IR, calculated from the ratio of the azlactone carbonyl (C=O) peak height (1822 cm⁻¹) to the carboxylic acid carbonyl (C=O) peak height (1734 cm⁻¹).

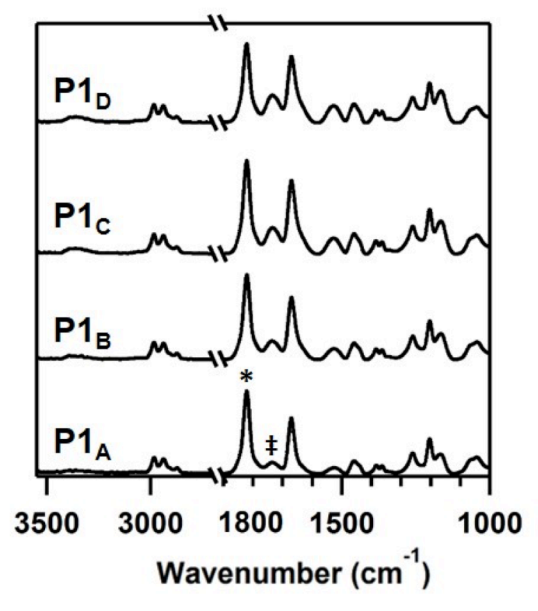


Figure 3. ATR IR spectra for partially hydrolyzed derivatives **P1**_A, **P1**_B, **P1**_C, and **P1**_D. The intensity of the azlactone carbonyl [denoted by (*); C=O, 1818 cm⁻¹] peak decreases relative to the intensity of the carboxylic acid carbonyl stretching [denoted by (‡); C=O, 1734 cm⁻¹] with increasing fraction of partial-hydrolysis from **P1**_A to **P1**_D; this ratio is provided for each polymer in Table 1.

quantitative ¹³C NMR spectroscopy. As shown in Table 1, the degree of partial hydrolysis ranged from 13.8% to 35.5% (analysis methods are described in the Materials and Methods section, and representative ¹³C NMR spectra are shown in Figure S2). Figure 3 shows representative IR spectra for these partially hydrolyzed polymers. These results show that as the percentage of hydrolysis increases (from **P1**_A to **P1**_D), the height of the azlactone carbonyl peak at 1821 cm⁻¹ decreases, and the carboxylic acid carbonyl peak at 1734 cm⁻¹ increases; the ratio of these two peak heights for polymers **P1**_A to **P1**_D are given in Table 1. We also note that, as the percentage of hydrolysis increased from **P1**_A to **P1**_D, evidence of the amide N-H bending mode (1528 cm⁻¹) became more pronounced.

Figure 4A shows digital pictures of PEI/PVDMA multilayers 35 bilayers thick fabricated using P1_A, P1_B, P1_C, and P1_D and iterative immersion protocols identical to those described above. An image of a PEI/P1 control film fabricated using pristine PVDMA is also shown for comparison. All of the films fabricated using the partially hydrolyzed derivatives were optically opaque and appeared rough to the naked eye, similar to the coatings described above using P1_X and shown in Figure 2C. However, the film fabricated using P1 (containing 0% hydrolyzed side chains) was again optically clear, visually smooth, and uniform. Figure 4B shows the results of analysis of the advancing water contact angles (θ) of multilayers fabricated using P1 and polymers P1_A, P1_B, P1_C, or P1_D. Black bars in Figure 4B show the water contact angles measured on as-fabricated (azlactone-containing) films; grey bars show contact angles measured after the functionalization of those reactive films by treatment with decylamine (20 mg/mL in THF, overnight), a hydrophobic amine used in past studies on the fabrication of nanoporous and superhydrophobic PEI/PVDMA coatings. ^{44,45,49,50} Representative images of water droplets contacting these surfaces are shown in Figure S4. Plots showing corresponding receding water

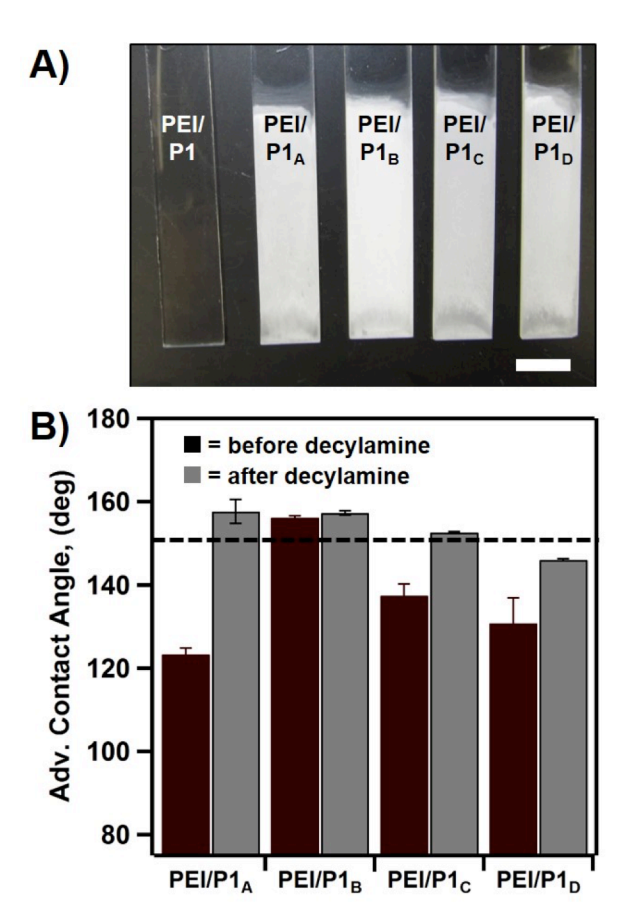


Figure 4. (A) Digital pictures showing the physical appearance of 35 bilayer thick PEI/P1 and PEI/P1_X films assembled on glass substrates. Scale bar = 1 cm. (B) Plot showing the advancing water contact angle measured on PEI/P1_X films fabricated using P1_A, P1_B, P1_C, and P1_D shown in part A. Water contact angles were measured before (black bars) and after functionalization with decylamine (grey bars; see text). The dotted line marks the contact angle of 150° commonly used as an indicator of superhydrophobicity (see text). Error bars represent the standard deviation of at least five measurements.

contact angles and associated values of contact angle hysteresis (defined as the difference in advancing and receding contact angles) are shown in Figure S5.

Films fabricated using $P1_A$, the derivative with the lowest degree of hydrolysis (13.8%), were the least hydrophobic, with $\theta = 123.4 \pm 1.4^{\circ}$, but became superhydrophobic after decylamine functionalization, $\theta = 157.7 \pm 2.9^{\circ}$ (superhydrophobicity is defined here as a surface

with a contact angle >150° and a contact angle hysteresis, or roll-off angle, of < 10°). 55,56 In contrast, PEI/P1_B films (16.7% hydrolyzed) were superhydrophobic both before ($\theta = 156.2 \pm$ 0.4°) and after functionalization ($\theta = 157.3 \pm 0.5^{\circ}$). PEI/P1_C films (25.9% hydrolyzed) exhibited similar wetting behaviors to PEI/P1_B films ($\theta = 137.5 \pm 2.7^{\circ}$ before, and $\theta = 152.6 \pm 0.2^{\circ}$ after functionalization). In contrast, PEI/P1p films (35.5% hydrolyzed) did not exhibit superhydrophobicity either before ($\theta = 130.8 \pm 6.1^{\circ}$) or after functionalization ($\theta = 146.0 \pm 0.3^{\circ}$). On the basis of these results, we conclude that (i) the number of carboxylic acid side chains present in the P1x derivatives has a significant influence on the wetting behaviors of these materials, and (ii) there is an apparent window of carboxylic acid content (between ~17% and ~25%) over which superhydrophobicity can be achieved after treatment with decylamine. Films fabricated using P1_X derivatives containing higher percentages of hydrolyzed side chain groups (e.g., P1_D, ~36% hydrolysis) were rough and optically opaque (Figure 4A), but not superhydrophobic either before or after decylamine functionalization. Moreover, we note that films fabricated using P1x derivatives with lower extents of hydrolysis (e.g., P1_A ~17% hydrolysis) exhibited superhydrophobicity even prior to functionalization with decylamine.

We next sought to characterize potential differences in film morphology exhibited by PEI/PVDMA films fabricated using P1, P1_A, P1_B, P1_C, and P1_D. Figure 5 shows top-down SEM images of the five films shown in Figure 4A. These images reveal PEI/P1 films to be uniformly smooth and largely featureless (Figure 5A), but that all other films assembled using P1_{A-D} exhibited more complex morphologies and many micro- and nanoscale topographic features that were not present in PEI/P1 films (Figure 5B-E). Further inspection of the images (see also the insets in these images) reveals qualitative differences in film morphology that vary with the percentages of hydrolysis in the P1_X derivatives used to fabricate the films. For example, films

fabricated using $P1_A$ and $P1_B$ (Figure 5B-C), which contain the lowest degrees of hydrolysis (~14% and ~17%, respectively) exhibit complex morphologies composed of surface-exposed nanoscale bumps, particles, and pores that are similar to features reported previously for many nanoporous and topographically rough PEI/PVDMA films that exhibit extreme non-wetting behaviors. 44,45,49,50 In contrast, inspection of the images in Figure 5D-E reveals films fabricated from polymers with higher percentages of hydrolysis ($P1_C$ and $P1_D$, with ~26% and ~36% hydrolysis, respectively) to have complex morphologies with qualitatively smoother surfaces, or a lack of readily observable hierarchical nanoscale features similar to those shown in Figure 5B-C.

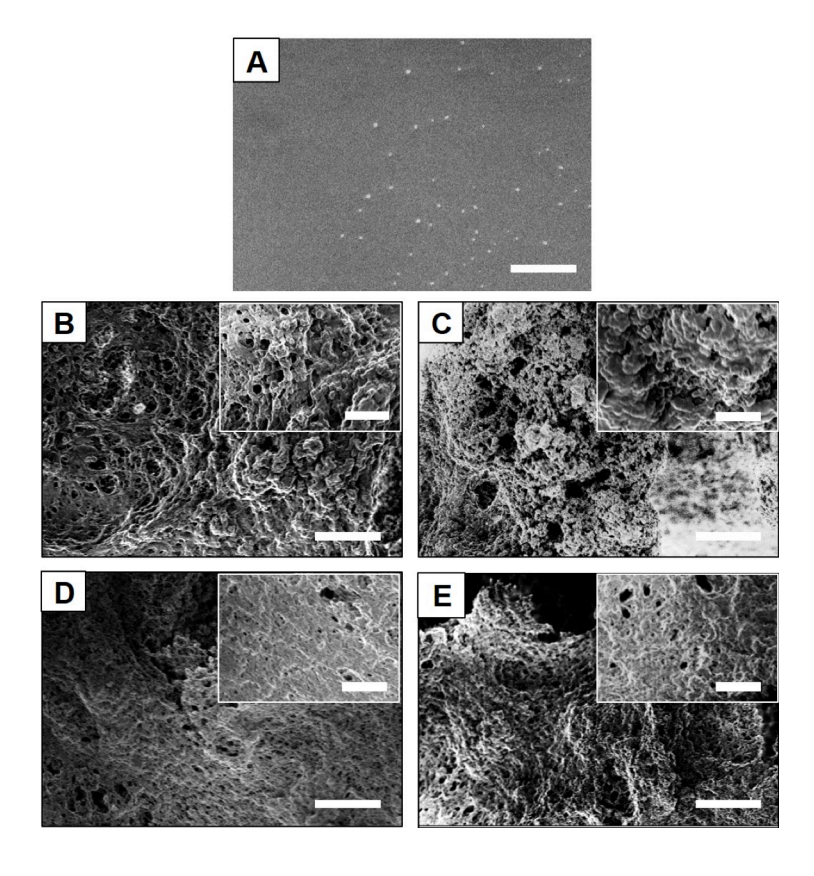


Figure 5. (A-E) SEM images showing the film morphology at the surfaces of 35 bilayer thick PEI/P1 and PEI/P1_X assembled on glass substrates. PEI/P1 films shown in (A) are largely featureless, while films assembled using (B) P1_A, (C) P1_B, (D) P1_C, and (E) P1_D exhibit more complex morphologies with many micro- and nanoscale features. Scale bar = 5 μ m; 2 μ m insets.

In combination with these qualitative characterization studies, we also used nitrogen gas adsorption analysis to determine whether differences in the sizes, void volumes, and surface areas of pores apparent in SEM images of films fabricated using P1x derivatives could be characterized quantitatively. These experiments revealed adsorption isotherms and the pore size distributions of films fabricated with hydrolyzed PVDMA to be different from those of films fabricated with unhydrolyzed PVDMA. However, these isotherms were generally complex and difficult to interpret with confidence using BET theory or other related models typically used for analysis of gas adsorption isotherms of porous materials. We speculate that these deviations from model behavior could arise, at least in part, from the morphologies of these materials, which, as suggested by the SEM images, contain pores that are interconnected, irregular, and have shapes and sizes outside the range typically considered appropriate or ideal for analysis using these methods. We are currently investigating other approaches to quantify differences in the porosities of these materials.

The apparent differences in morphology and nanoscale topographic features shown in Figure 5 could account for the lower water contact angles observed for the PEI/P1_C and PEI/P1_D films shown in Figure 4B (black bars). Taken together, these results hint that the influence of side chain hydrolysis on the wetting behaviors of these coatings could arise, at least in part, from the influence of carboxylic acid groups on the nanoscale morphologies that evolve during assembly. We consider it likely that differences in the number of hydrophilic carboxylic acid groups present in these films could also play an important role in defining the wetting properties of these materials. Ultimately, the wetting behaviors of these films, as defined by the contact angle measurements reported here, are likely to be a result of the interplay of the influences of both morphology and surface energy.

Figure 6 shows ATR IR spectra of PEI/PVDMA films fabricated using $P1_A$, $P1_B$, $P1_C$, and $P1_D$ prior to treatment with decylamine. Inspection of these images reveals the presence of unreacted azlactone functionality (e.g., the azlactone carbonyl peak at 1821 cm⁻¹), and that the carboxylic acid carbonyl peak observed in the IR spectra of polymers using $P1_A$, $P1_B$, $P1_C$, and $P1_D$ is absent (C=O 1734 cm⁻¹; see Figure 3). Because PEI contains basic primary, secondary, and tertiary amine functionality, it is likely that the carboxylic acid groups in these films could be deprotonated and, thus, present in the carboxylate form. The spectra shown in Figure 6 tend to support this conclusion because the hydrolyzed azlactone carboxylic acid stretch observed for $P1_X$ is absent (see Figure 3). However, the anticipated carboxylate carbonyl stretch (reported at \sim 1645 cm⁻¹ for cross-linked polymer beads containing fully-hydrolyzed VDMA in the sodium

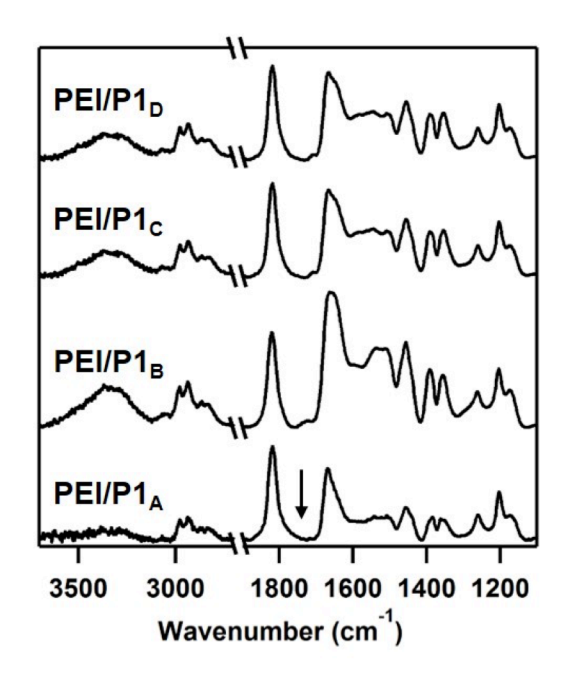


Figure 6. ATR IR spectra for 35 bilayer thick PEI/P1_X films assembled on glass substrates using partially hydrolyzed derivatives P1_A, P1_B, P1_C, and P1_D. The black arrow indicates the expected position of the carboxylic acid carbonyl stretching (C=O, 1734 cm⁻¹, based on the IR spectra of the individual polymers prior to assembly; see Figure 1).

salt form)^{54,57} is obscured by the overlapping amide carbonyl stretch and azlactone imine peaks that are centered at ~1664 cm⁻¹. Although the results shown in Figure 6 are not definitive proof of ion-pairing interactions between carboxylic acid and amine functionality in these films, these results are generally consistent with that possibility. We return again in the discussion below to the potential influence of such ion-pairing interactions on the growth and evolution of nanoscale morphology that occurs during the assembly of these materials.

Consideration of the influence of partial side chain hydrolysis on evolution of film morphology

The nanoscale structures and porous morphologies shown in Figure 5B-C and reported in past studies could arise during fabrication from the formation of nanoscale aggregates of PEI and PVDMA. We hypothesized that these features could arise either (i) in solution and prior to contact with the surface to be coated (in this scenario, film growth could occur, at least in part, by the deposition of preformed, solution-phase PEI-PVDMA nano-aggregates), or (ii) upon the deposition of either PEI or PVDMA on the surface of a growing film during individual steps in the fabrication cycle (in this scenario, these features would result from transformations that occur at the surface, or possibly within the bulk, of a growing film as each new polymer 'layer' is deposited). We note that it is also possible that these morphologies could arise during other steps of the fabrication process, including at points during which film-coated substrates are removed from polymer or rinse solutions and transported to the following solution. At these points in the process, for example, brief exposure to air or physical transformations promoted by the evaporation of acetone could potentially lead to film reorganization and the evolution of complex morphologies. Other possibilities may also exist that are not considered here. It is clear from visual inspection and physicochemical characterization of these films during fabrication,

however, that these morphologies develop and evolve during the fabrication process, and that nanoscale roughness and porosity do not arise as a consequence of transformations that occur after film assembly is complete (e.g., upon final drying or upon long-term storage, etc.).

The first hypothesis described above is supported generally by the observation that both the polymer solutions and primary rinse baths used during fabrication often become visually cloudy during fabrication, consistent with the formation of polymer aggregates in these solutions as film fabrication progresses. This phenomenon could arise from carryover of polymer into and between solutions during the iterative transfer of substrates from solution to solution during fabrication; see Figure 2A. (We note that solutions of PEI or PVDMA alone do not flocculate or yield visible precipitates upon standing on the time scales used for film fabrication). To provide insight into the potential role of aggregates in the evolution of nanostructure in these materials during fabrication, we conducted a series of experiments using acetone solutions of PEI and a model P1_x polymer containing 22.5± 1.4% hydrolyzed groups. Characterization of PEI/PVDMA films fabricated using this polymer by ellipsometry, SEM, FTIR, and contact angle measurements revealed the influence of this polymer on film growth and morphology to be similar to that of P1_C; see discussion below.

Figure 7 shows SEM images of samples of polymer solution (A: PEI solution; B: $P1_X$ solution) and the rinse baths (C: first rinse vial after immersion in PEI solution; D: first rinse vial after immersion in $P1_X$ solution) collected after the fabrication of a 35 bilayer PEI/PVDMA film (these solutions were drop-cast onto silicon and acetone was evaporated prior to imaging; see Materials and Methods). Inspection of these images reveals the presence of microscale and nanoscale aggregates. Although it is not possible to infer from these results anything regarding the compositions of these aggregates or their sizes before drying, the aggregates in these images

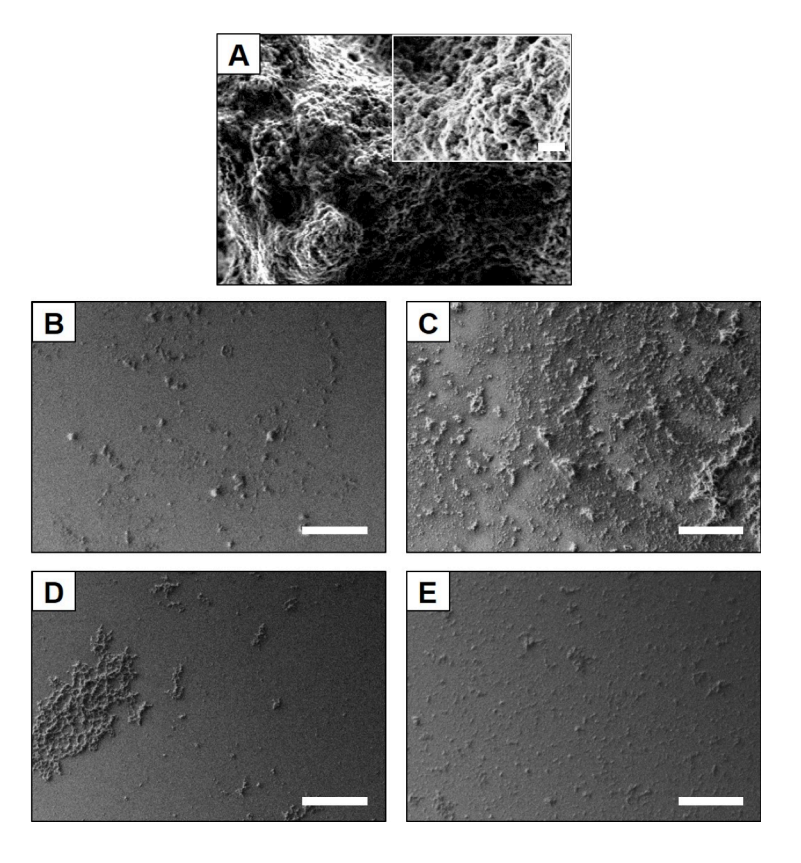


Figure 7. (A) SEM image showing the morphology of a 35 bilayer thick PEI/P1_X film assembled on a glass substrate using a model P1_X with 22.5 ± 1.4 percent hydrolysis. (B) and (C) show SEM images of polymer aggregates present in the dried samples of PEI and P1_X film fabrication solutions, respectively, collected after film assembly. (D) and (E) show SEM images of polymer aggregates present in the first PEI and first P1_X acetone rinse vials used for film fabrication, respectively, collected after film assembly (see text). Scale bar = 5 μ m; 1 μ m insets.

are consistent with the visible presence of polymer aggregates in these solutions during and after fabrication. More generally, these observations suggest that the nanoscale structures in the PEI/PVDMA films discussed above could potentially arise from the deposition or reaction of these aggregates onto surfaces during immersion at each step in the film fabrication process.

The results of additional control experiments in which films were fabricated using a modified rinse procedure suggested that nanoscale structure and morphology can also evolve

during fabrication even when polymer aggregates are not substantially present in solution. In this modified procedure, rinse solutions were replaced with fresh acetone during fabrication after every single rinse step to prevent the accumulation and carryover of PEI or P1_x during successive immersions (all other fabrication parameters were otherwise identical). The images in Figure 8D and 8E show SEM images of the PEI and P1_x solutions used in these experiments. Relative to Figure 7, these images reveal the absence of nanoscale or microscale aggregates, demonstrating that this modified rinse protocol was sufficient to prevent polymer carryover and in-process aggregate formation in these solutions. Figure 8C, however, shows an SEM image of a 35-bilayer film fabricated using this modified protocol, and reveals the presence of significant nanoscale structure and texture on the surface of the film. Likewise, Figure 8A shows an image of a film fabricated under similar conditions, and reveals the film to be visually rough and opaque, albeit not as visually rough or as opaque as films shown in Figure 4.

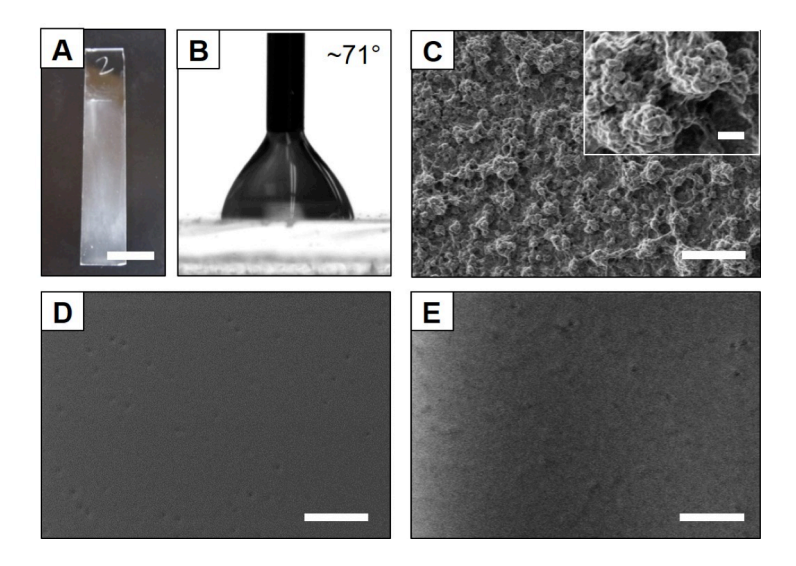


Figure 8. Characterization of a 35 bilayer thick film fabricated using a model $P1_X$ with 22.5 ± 1.4 percent hydrolysis by changing the acetone rinse solutions after every rinse step (see text). (A) Digital picture showing the physical appearance of the film; scale bar = 1 cm. (B) Water contact angle analysis demonstrating that the film was readily wet by water. (C) SEM image showing the morphology at the surface of the film. (D) and (E) show SEM images indicating the absence of polymer aggregates in the PEI and $P1_X$ film fabrication solutions, respectively, collected after film assembly (see text). Scale bars in (C-E) = 5 µm; 1 µm insets.

When combined, these results demonstrate that micro- and nanoscale features are able to form on the surfaces of growing films during the deposition of PEI or PVDMA in ways that can occur independent of the formation and possible deposition of solution-based polymer aggregates. We note again, however, that films fabricated by this modified procedure are visually different (Figure 8A), and results shown in Figure 8B also demonstrate the contact angles of these films to be significantly less hydrophobic ($\theta \sim 71^{\circ}$) than films made by the more conventional fabrication protocol. On the basis of these results and observations, it is thus also possible that the formation and subsequent deposition of polymer aggregates in solution during fabrication could also play a role and lead to, for example, a more rapid onset of surface features that promote the generation of roughness and porosity. Additional experiments will be required to probe these possibilities more completely and characterize factors that influence the formation

of nanostructure under conditions where the potential for the aggregation of PEI and PVDMA in solution is minimized or completely eliminated. Experiments conducted using PEI and PVDMA solutions containing acetone-soluble salts that could potentially screen ionic interactions between these polymers lead to other complex film growth profiles that we were unable to clearly or reliably interpret in this context. Those preliminary results suggest, however, that the addition of small-molecules salts and electrolytes to polymer solutions could provide other interesting opportunities to tune the structures and behaviors of these PEI/PVDMA films. Additional studies to explore the potential of this, and other related approaches, are currently underway and will be reported in due course.

Summary and Conclusions

Our results demonstrate that the presence of hydrolyzed azlactone groups in PVDMA can substantially influence the growth and resulting morphologies of multilayer films fabricated by reactive LbL assembly. Whereas unhydrolyzed PVDMA and PEI yield thin films that are smooth, transparent, and largely devoid of micro- and nanoscale features, films assembled using partially hydrolyzed PVDMA are generally thick, porous, and exhibit substantial roughness together with micro- and nanoscale topographic features. The morphologies and wetting behaviors of these films are, in general, similar to those of nanoporous and topographically complex PEI/PVDMA coatings reported in past studies. The results reported here also demonstrate that the degree of azlactone hydrolysis can influence the surface properties and interfacial behaviors of films, and suggest that carboxylic acid side chain groups could participate in acid/base and ionic interactions that could also influence structure formation and film growth. The mechanism of structure formation and the evolution of roughness and porosity

in these materials is not yet completely understood. However, our results provide new and useful

insights into molecular-level features that can influence the properties and behaviors of these

materials, and introduce well-defined approaches that can be used to achieve these morphologies

reliably and reproducibly. The work reported here thus provides guidance that should prove

useful for further tuning the porosities and tailoring the physicochemical behaviors of these

reactive coatings in ways that are important in applied contexts.

Acknowledgments. This work was supported by the NSF through grants to the UW-Madison

Materials Research Science and Engineering Center (MRSEC; DMR-1720415) and the UW-

Madison Nanoscale Science and Engineering Center (NSEC; DMR-0832760), and by the Office

of Naval Research (N00014-16-1-2185), and made use of NSF-supported facilities (DMR-

1720415, DMR-0832760, and CHE-1048642). We thank Dr. Charles Fry for assistance with

quantitative ¹³C NMR spectroscopy experiments. M.C.D.C. acknowledges the Natural Sciences

Engineering Research Council of Canada for a graduate fellowship.

Supporting Information. Additional spectroscopic characterization of polymers and

physicoshemical characterization of polymer-based coatings (PDF). This material is available

free of charge via the Internet.

ORCID

David M. Lynn: 0000-0002-3140-8637

Matthew C. D. Carter: 0000-0003-1678-2636

29

References

- 1. Zelikin, A. N., Drug Releasing Polymer Thin Films: New Era of Surface-Mediated Drug Delivery. *ACS Nano* **2010**, *4* (5), 2494-2509.
- 2. Kaur, P.; Hupp, J. T.; Nguyen, S. T., Porous Organic Polymers in Catalysis: Opportunities and Challenges. *ACS Catalysis* **2011**, *1* (7), 819-835.
- 3. Pavlukhina, S.; Sukhishvili, S., Polymer assemblies for controlled delivery of bioactive molecules from surfaces. *Adv. Drug Delivery Rev.* **2011**, *63* (9), 822-836.
- 4. Wu, D.; Xu, F.; Sun, B.; Fu, R.; He, H.; Matyjaszewski, K., Design and Preparation of Porous Polymers. *Chem. Rev.* **2012**, *112* (7), 3959-4015.
- 5. Joseph, N.; Ahmadiannamini, P.; Hoogenboom, R.; Vankelecom, I. F. J., Layer-by-layer preparation of polyelectrolyte multilayer membranes for separation. *Polym. Chem.* **2014**, *5* (6), 1817-1831.
- 6. Chaoui, N.; Trunk, M.; Dawson, R.; Schmidt, J.; Thomas, A., Trends and challenges for microporous polymers. *Chem. Soc. Rev.* **2017**, *46* (11), 3302-3321.
- 7. Tan, L.; Tan, B., Hypercrosslinked porous polymer materials: design, synthesis, and applications. *Chem. Soc. Rev.* **2017**, *46* (11), 3322-3356.
- 8. Wu, J.; Xu, F.; Li, S.; Ma, P.; Zhang, X.; Liu, Q.; Fu, R.; Wu, D., Porous Polymers as Multifunctional Material Platforms toward Task-Specific Applications. *Adv. Mater.* **2019**, *31* (4), 1802922.
- 9. Mendelsohn, J. D.; Barrett, C. J.; Chan, V. V.; Pal, A. J.; Mayes, A. M.; Rubner, M. F., Fabrication of microporous thin films from polyelectrolyte multilayers. *Langmuir* **2000**, *16* (11), 5017-5023.
- 10. Fery, A.; Schöler, B.; Cassagneau, T.; Caruso, F., Nanoporous Thin Films Formed by Salt-Induced Structural Changes in Multilayers of Poly(acrylic acid) and Poly(allylamine). *Langmuir* **2001**, *17* (13), 3779-3783.
- 11. Hiller, J.; Mendelsohn, J. D.; Rubner, M. F., Reversibly erasable nanoporous anti-reflection coatings from polyelectrolyte multilayers. *Nat. Mater.* **2002**, *1* (1), 59-63.
- 12. Zhai, L.; Cebeci, F. C.; Cohen, R. E.; Rubner, M. F., Stable superhydrophobic coatings from polyelectrolyte multilayers. *Nano Lett.* **2004**, *4* (7), 1349-1353.
- 13. Sui, Z. J.; Schlenoff, J. B., Phase separations in pH-responsive polyelectrolyte multilayers: Charge extrusion versus charge expulsion. *Langmuir* **2004**, *20* (14), 6026-6031.

- 14. Lowman, G. M.; Tokuhisa, H.; Lutkenhaus, J. L.; Hammond, P. T., Novel solid-state polymer electrolyte consisting of a porous layer-by-layer polyelectrolyte thin film and oligoethylene glycol. *Langmuir* **2004**, *20* (22), 9791-9795.
- 15. Berg, M. C.; Zhai, L.; Cohen, R. E.; Rubner, M. F., Controlled drug release from porous polyelectrolyte multilayers. *Biomacromolecules* **2006**, *7* (1), 357-364.
- 16. Cebeci, F. C.; Wu, Z. Z.; Zhai, L.; Cohen, R. E.; Rubner, M. F., Nanoporosity-driven superhydrophilicity: A means to create multifunctional antifogging coatings. *Langmuir* **2006**, *22* (6), 2856-2862.
- 17. Zhai, L.; Berg, M. C.; Cebeci, F. C.; Kim, Y.; Milwid, J. M.; Rubner, M. F.; Cohen, R. E., Patterned superhydrophobic surfaces: Toward a synthetic mimic of the Namib Desert beetle. *Nano Lett.* **2006**, *6* (6), 1213-1217.
- 18. Olugebefola, S. C.; Kuhlman, W. A.; Rubner, M. F.; Mayes, A. M., Photopatterned Nanoporosity in Polyelectrolyte Multilayer Films. *Langmuir* **2008**, *24* (9), 5172-5178.
- 19. Hajicharalambous, C. S.; Lichter, J.; Hix, W. T.; Swierczewska, M.; Rubner, M. F.; Rajagopalan, P., Nano- and sub-micron porous polyelectrolyte multilayer assemblies: Biomimetic surfaces for human corneal epithelial cells. *Biomaterials* **2009**, *30* (23), 4029-4036.
- 20. Li, Y.; Li, L.; Sun, J., Bioinspired Self-Healing Superhydrophobic Coatings. *Angew. Chem., Int. Ed.* **2010**, *49* (35), 6129-6133.
- 21. Kim, D.; Tzeng, P.; Barnett, K. J.; Yang, Y.-H.; Wilhite, B. A.; Grunlan, J. C., Highly Size-Selective Ionically Crosslinked Multilayer Polymer Films for Light Gas Separation. *Adv. Mater.* **2014**, *26* (5), 746-751.
- 22. Sung, C.; Ye, Y.; Lutkenhaus, J. L., Reversibly pH-Responsive Nanoporous Layer-by-Layer Microtubes. *ACS Macro Letters* **2015**, *4* (4), 353-356.
- 23. Yu, J.; Sanyal, O.; Izbicki, A. P.; Lee, I., Development of Layered Multiscale Porous Thin Films by Tuning Deposition Time and Molecular Weight of Polyelectrolytes. *Macromol. Rapid Commun.* **2015**, *36* (18), 1669-1674.
- 24. Ziminska, M.; Dunne, N.; Hamilton, A. R., Porous Materials with Tunable Structure and Mechanical Properties via Templated Layer-by-Layer Assembly. *ACS Appl. Mater. Interfaces* **2016**, *8* (34), 21968-21973.
- 25. DuChanois, R. M.; Epsztein, R.; Trivedi, J. A.; Elimelech, M., Controlling pore structure of polyelectrolyte multilayer nanofiltration membranes by tuning polyelectrolyte-salt interactions. *J. Membr. Sci.* **2019**, *581*, 413-420.
- 26. Hammond, P. T., Form and Function in Multilayer Assembly: New Applications at the Nanoscale. *Adv. Mater.* **2004**, *16* (15), 1271-1293.

- 27. Quinn, J. F.; Johnston, A. P. R.; Such, G. K.; Zelikin, A. N.; Caruso, F., Next generation, sequentially assembled ultrathin films: beyond electrostatics. *Chem. Soc. Rev.* **2007**, *36* (5), 707-718.
- 28. Decher, G., Layer-by-Layer Assembly (Putting Molecules to Work). In *Multilayer Thin Films: Sequential Assembly of Nanocomposite Materials, 2nd Edition*, Decher, G. and Schlenoff, J. B., Eds. Wiley-VCH: Weinheim, Germany; 2012; pp 1-21.
- 29. Borges, J.; Mano, J. F., Molecular Interactions Driving the Layer-by-Layer Assembly of Multilayers. *Chem. Rev.* **2014**, *114* (18), 8883-8942.
- 30. Richardson, J. J.; Björnmalm, M.; Caruso, F., Technology-driven layer-by-layer assembly of nanofilms. *Science* **2015**, *348* (6233).
- 31. Xiao, F.-X.; Pagliaro, M.; Xu, Y.-J.; Liu, B., Layer-by-layer assembly of versatile nanoarchitectures with diverse dimensionality: a new perspective for rational construction of multilayer assemblies. *Chem. Soc. Rev.* **2016**, *45*, 3088-3121.
- 32. Zacharia, N. S.; DeLongchamp, D. M.; Modestino, M.; Hammond, P. T., Controlling Diffusion and Exchange in Layer-by-Layer Assemblies. *Macromolecules* **2007**, *40* (5), 1598-1603.
- 33. Zacharia, N. S.; Modestino, M.; Hammond, P. T., Factors Influencing the Interdiffusion of Weak Polycations in Multilayers. *Macromolecules* **2007**, *40* (26), 9523-9528.
- 34. Gilbert, J. B.; Rubner, M. F.; Cohen, R. E., Depth-profiling X-ray photoelectron spectroscopy (XPS) analysis of interlayer diffusion in polyelectrolyte multilayers. *Proc. Natl. Acad. Sci. U. S. A.* **2013**, *110* (17), 6651-6656.
- 35. Nolte, A. J.; Takane, N.; Hindman, E.; Gaynor, W.; Rubner, M. F.; Cohen, R. E., Thin Film Thickness Gradients and Spatial Patterning via Salt Etching of Polyelectrolyte Multilayers. *Macromolecules* **2007**, *40* (15), 5479-5486.
- 36. Nolte, A. J.; Treat, N. D.; Cohen, R. E.; Rubner, M. F., Effect of Relative Humidity on the Young's Modulus of Polyelectrolyte Multilayer Films and Related Nonionic Polymers. *Macromolecules* **2008**, *41* (15), 5793-5798.
- 37. Bernards, D. A.; Desai, T. A., Nanoscale porosity in polymer films: fabrication and therapeutic applications. *Soft Matter* **2010**, *6* (8), 1621-1631.
- 38. Li, Y.; Wang, X.; Sun, J., Layer-by-layer assembly for rapid fabrication of thick polymeric films. *Chem. Soc. Rev.* **2012**, *41* (18), 5998-6009.
- 39. Richardson, J. J.; Cui, J.; Björnmalm, M.; Braunger, J. A.; Ejima, H.; Caruso, F., Innovation in Layer-by-Layer Assembly. *Chem. Rev.* **2016**, *116* (23), 14828-14867.

- 40. An, Q.; Huang, T.; Shi, F., Covalent layer-by-layer films: chemistry, design, and multidisciplinary applications. *Chem. Soc. Rev.* **2018**, *47* (13), 5061-5098.
- 41. Buck, M. E.; Zhang, J.; Lynn, D. M., Layer-by-Layer Assembly of Reactive Ultrathin Films Mediated by Click-Type Reactions of Poly(2-Alkenyl Azlactone)s. *Adv. Mater.* **2007**, *19* (22), 3951-3955.
- 42. Broderick, A. H.; Azarin, S. M.; Buck, M. E.; Palecek, S. P.; Lynn, D. M., Fabrication and Selective Functionalization of Amine-Reactive Polymer Multilayers on Topographically Patterned Microwell Cell Culture Arrays. *Biomacromolecules* **2011**, *12* (6), 1998-2007.
- 43. Broderick, A. H.; Carter, M. C. D.; Lockett, M. R.; Smith, L. M.; Lynn, D. M., Fabrication of Oligonucleotide and Protein Arrays on Rigid and Flexible Substrates Coated with Reactive Polymer Multilayers. *ACS Appl. Mater. Interfaces* **2013**, *5* (2), 351-359.
- 44. Buck, M. E.; Schwartz, S. C.; Lynn, D. M., Superhydrophobic Thin Films Fabricated by Reactive Layer-by-Layer Assembly of Azlactone-Functionalized Polymers. *Chem. Mater.* **2010**, *22* (23), 6319-6327.
- 45. Manna, U.; Lynn, D. M., Synthetic Surfaces with Robust and Tunable Underwater Superoleophobicity. *Adv. Funct. Mater.* **2015**, *25* (11), 1672-1681.
- 46. Manna, U.; Raman, N.; Welsh, M. A.; Zayas-Gonzalez, Y. M.; Blackwell, H. E.; Palecek, S. P.; Lynn, D. M., Slippery Liquid-Infused Porous Surfaces that Prevent Microbial Surface Fouling and Kill Non-Adherent Pathogens in Surrounding Media: A Controlled Release Approach. *Adv. Funct. Mater.* **2016**, *26* (21), 3599-3611.
- 47. Carter, M. C. D.; Lynn, D. M., Covalently Crosslinked and Physically Stable Polymer Coatings with Chemically Labile and Dynamic Surface Features Fabricated by Treatment of Azlactone-Containing Multilayers with Alcohol-, Thiol-, and Hydrazine-Based Nucleophiles. *Chem. Mater.* **2016**, *28* (14), 5063-5072.
- 48. Manna, U.; Zayas-Gonzalez, Y. M.; Carlton, R. J.; Caruso, F.; Abbott, N. L.; Lynn, D. M., Liquid Crystal Chemical Sensors That Cells Can Wear. *Angew. Chem., Int. Ed.* **2013,** *52* (52), 14011-14015.
- 49. Manna, U.; Kratochvil, M. J.; Lynn, D. M., Superhydrophobic Polymer Multilayers that Promote the Extended, Long-Term Release of Embedded Water-Soluble Agents. *Adv. Mater.* **2013**, *25* (44), 6405-6409.
- 50. Manna, U.; Broderick, A. H.; Lynn, D. M., Chemical Patterning and Physical Refinement of Reactive Superhydrophobic Surfaces. *Adv. Mater.* **2012**, *24* (31), 4291-4195.
- 51. Gardner, C. M.; Stöver, H. D. H., Reactive Polyanions Based on Poly(4,4-dimethyl-2-vinyl-2-oxazoline-5-one-co-methacrylic acid). *Macromolecules* **2011**, *44* (18), 7115-7123.

- 52. Heilmann, S. M.; Moren, D. M.; Krepski, L. R.; Rasmussen, J. K.; Gaddam, B. N.; Roscoe, S. B.; Lewandowski, K. M.; McIntosh, L. H.; Roberts, R. R.; Fansler, D. D.; Szekely, G. G.; Weil, D. A.; Thakur, K. A.; Pathre, S. V.; Battiste, J. L.; Hanggi, D. A., The Chemistry of 2-Alkenyl-5(4H)-Oxazolones. IX. Acid-Catalyzed Oligomerization. *J. Macromol. Sci., Part A: Pure Appl. Chem.* **2003**, *40* (8), 755-790.
- 53. Carter, M. D. C.; Jennings, J.; Speetjens, F. W., II; Mahanthappa, M. K.; Lynn, D. M., A Reactive Platform Approach for the Rapid Synthesis and Discovery of High *X*/Low N Block Polymers. *Macromolecules* **2016**, *49*, 6268-6276.
- 54. Heilmann, S. M.; Rasmussen, J. K.; Krepski, L. R., Chemistry and technology of 2-alkenyl azlactones. *J. Polym. Sci., Part A: Polym. Chem.* **2001**, *39* (21), 3655-3677.
- 55. Wang, S.; Liu, K.; Yao, X.; Jiang, L., Bioinspired Surfaces with Superwettability: New Insight on Theory, Design, and Applications. *Chem. Rev.* **2015**, *115* (16), 8230-8293.
- 56. Wen, L.; Tian, Y.; Jiang, L., Bioinspired Super-Wettability from Fundamental Research to Practical Applications. *Angew. Chem., Int. Ed.* **2015**, *54* (11), 3387-3399.
- 57. Rasmussen, J. K.; Heilmann, S. M.; Krepski, L. R.; Jensen, K. M.; Mickelson, J.; Johnson, K., Crosslinked, hydrophilic, azlactone-functional polymeric beads: a two-step approach. *React. Polym.* **1992**, *16* (2), 199-212.

For Table of Contents Use Only:

